Remote Sensing Letters

ISSN: (Print) (Online) Journal homepage: www.tandfonline.com/journals/trsl20

Single photon lidar signal attenuation under boreal forest conditions

Liam Irwin, Nicholas C. Coops, Martin Queinnec, Grant McCartney & Joanne C. White

To cite this article: Liam Irwin, Nicholas C. Coops, Martin Queinnec, Grant McCartney & Joanne C. White (2021) Single photon lidar signal attenuation under boreal forest conditions, Remote Sensing Letters, 12:10, 1049-1060, DOI: 10.1080/2150704X.2021.1962575

To link to this article: https://doi.org/10.1080/2150704X.2021.1962575

Published online: 24 Aug 2021.

REMOTE SENSING LETTERS
2021, VOL. 12, NO. 10, 1049–1060
https://doi.org/10.1080/2150704X.2021.1962575

Taylor & Francis
Taylor & Francis Group

Single photon lidar signal attenuation under boreal forest conditions

Liam Irwin[a], Nicholas C. Coops[a], Martin Queinnec[a], Grant McCartney[b] and Joanne C. White[c]

[a]Department of Forest Resources Management, University of British Columbia, Vancouver, British Columbia, Canada; [b]Forest Information Systems, Rayonier Advanced Materials, Timmins, Ontario, Canada; [c]Canadian Forest Service (Pacific Forestry Centre), Natural Resources Canada, Victoria, British Columbia, Canada

ABSTRACT

Single-photon lidar (SPL100) is a recently commercialized airborne lidar system facilitating efficient wide-area acquisitions of high-density point clouds due to its capacity for higher altitude acquisitions compared to traditional linear-mode lidar (LML) systems. Increased acquisition efficiency and point densities make SPL100 attractive for forest management applications. SPL100 utilizes 532 nm (green wavelength) lasers, wherein there is reduced reflectance from vegetation, increased sensitivity to solar noise, and increased signal attenuation, which may impact the vertical distribution of SPL100 returns in forest canopies. We assessed SPL100 data acquisitions over managed forests in north-eastern Ontario, Canada, using high-density unmanned aerial vehicle-borne laser scanning (ULS) data as reference over a range of forest conditions with variable vertical structure. Signal attenuation depth of individual SPL100 returns was estimated through a surface model normalization approach stratified by a ULS-derived structural index that compared densities of returns in the upper canopy to low vegetation and near ground. Canopy signal attenuation was closely matched in both systems, particularly in the upper canopy and near the ground surface; however, results showed a 31% reduction in the relative characterization of mid-canopy vegetation layers by SPL100 under conditions identified by the structural index as closed canopy, compared to the ULS system.

ARTICLE HISTORY
Received 17 May 2021
Accepted 27 July 2021

1. Introduction

The Leica SPL100 is a single-photon light detection and ranging (lidar) sensor that enables increased spatial coverage and higher point density products when compared to conventional linear mode lidar (LML) systems (Stoker et al. 2016; Swatantran et al. 2016). SPL100 utilizes a 10 × 10 array to split emitted laser pulses into 100 low-powered 'beamlets'. Returning beamlet photons are captured by a highly sensitive 10 × 10 array of detectors that are capable of recording returned energy from single photons. Unlike most vegetation and terrain focused LML systems that emit pulses of near-infrared

CONTACT Liam Irwin liamakirwin@gmail.com Department of Forest Resources Management, University of British Columbia, 2424 Main Mall, Vancouver, British Columbia, V6T 1Z4, Canada

radiation (NIR), SPL100 utilizes 532 nm (green) wavelength lasers (Leica 2021). Green photons are more readily absorbed by photosynthetic foliar surfaces (e.g. leaves) than NIR; increasing signal attenuation, decreasing transmission through canopy layers and reducing the number and strength of return signals to the sensor (Hopkinson et al. 2016). These wavelengths are also vulnerable to effects of atmospheric scattering and solar noise (Wästlund et al. 2018; Degnan 2016). These differences have the potential to limit the ability of SPL100 pulses to penetrate certain dense vegetative cover configurations which may impact derivation of sub-canopy structure and accurate characterization of underlying ground surfaces in forested areas compared to conventional LML systems (White et al. 2021a).

Herein we compare the lidar signal attenuation of a SPL100 sensor, to a small-footprint conventional NIR wavelength, LML system mounted on an unmanned aerial vehicle (hereafter referred to as ULS) with the aim to characterize boreal forest vertical foliage profiles under a variety of vertical forest conditions. To do so, we stratify vertical forest foliage profiles, derived from the ULS system, across a range of boreal forest structures. We utilize a lidar signal attenuation approach to approximate the effective penetrative capacity of each sensor across the sites with the aim of improving our understanding of how SPL100 quantifies lower canopy information, and subsequent implications for use of these data for forest management applications.

2. Methods

2.1. Study area

The northern boreal Romeo Malette forest (RMF) located in north eastern Ontario, is characterized by relatively flat terrain and a continental climate with long winters, and short summers. Common forest compositions include naturally regenerated stands following harvest or natural disturbance composed of deciduous overstory species such as trembling aspen (*Populous tremuloidis)* and paper birch (*Betula papyrifera*), and mature; coniferous stands dominated by black spruce (*Picea mariana*), white spruce (*Picea glauca*), and eastern white cedar (*Thuja occidentalis*). Mixed wood multi-layer stands are characterized by dominant aspen overstories with understory layers of regenerating coniferous and deciduous species.

2.2. Ground plot composition

We established five representative 400 m^2 circular plots (11.28 m radius) at the centre of each lidar acquisition across common forest structure and species compositions present in the RMF. Field technicians collected a range of tree attribute information for all trees exceeding a 7.1 cm diameter at breast height threshold (Table 1).

2.3. Lidar acquisitions

2.3.1. Single photon lidar (SPL100)

SPL100 data was acquired as part of a large-scale acquisition in summer of 2018, at a nominal altitude of 3660 m above ground level, with 50% overlap between flight

Table 1. Summary of plot level field and lidar derived metrics. Diameter at breast height (dbh) refers to mainstem diameter measured at 1.3 m height; expressed as average and standard deviation of sample trees, configuration refers to qualitative description of plot structure based on field assessment and inspection of point clouds, structural index derived from ULS is defined in Section 2.5 and given as a mean value and standard deviation (SD), ULS and SPL100 density refer to the mean number of returns per square metre across acquisition areas by respective lidar systems, Percentage of lidar first returns ≥2 m in height indicates canopy cover metric for each platform. Signal attenuation quantiles refer to depth within canopy of returns within sample plot point clouds calculated as described in Section 2.6.

Attribute	Plot 1	Plot 2	Plot 3	Plot 4	Plot 5
Dominant Species	Paper Birch	Trembling Aspen	Trembling Aspen	Eastern white cedar	Black spruce
Tree diameter at breast height (cm) (mean (SD))	8.4 (1.7)	26.3 (9.6)	29.0 (14.8)	17.7 (9.5)	16.0 (5.0)
Configuration	Dense closed deciduous canopy	Mixed multi-layer open canopy	Mixed multi-layer open canopy	Dense closed coniferous canopy	Open coniferous canopy
Structural Index (mean (SD))	−0.79 (0.31)	−0.19 (0.52)	−0.18 (0.57)	−0.75 (0.35)	−0.17 (0.58)
SPL Density (points/m^2)	32	74	83	34	34
ULS Density (points/m^2)	1121	1372	1257	1350	1213
ULS First Returns ≥2 m (%)	98.5	95.8	90.9	98.2	76.6
SPL First Returns ≥2 m (%)	99.2	86.9	82.9	97.5	67.5
ULS Signal Attenuation Depth Quantiles (m) (25th, 50th, 95th)	0.5, 0.9, 7.2	0.6, 1.9, 28.8	0.7, 20.9, 31.7	0.6, 3.2, 9.8	0.9, 2.6, 15.7
SPL Signal Attenuation Depth Quantiles (m) (25th, 50th, 95th)	0.2, 0.5, 1.8	0.5, 15.0, 29.1	0.7, 5.2, 32.4	0.2, 0.8, 7.3	0.2, 1.4, 15.9

lines, at a pulse repetition frequency of 60 kHz, and a 30° field of view. These parameters resulted in an average return density of 44 points/m^2. Solar noise was removed by the data provider following the approach detailed in Gluckman (2016).

2.3.2. UAV-borne laser scanning (ULS)

In order to provide a baseline reference of vertical forest structure from a high density conventional LML system, ULS acquisitions were conducted over the plots in August, 2019 using a Phoenix AL3-32 system operating at 905 nm mounted on a DJI M600 Hexacopter UAV. Data was acquired at an altitude of 60 m above ground level ensuring at least 40% overlap between flight lines. ULS point density across the five areas of interest averaged 1264 points/m^2, totalling 9.44 hectares of lidar coverage.

2.4. Surface and canopy height model generation

Both SPL100 and ULS datasets were clipped to 80 m radius circles (20,000 m^2) surrounding sample plot centres and, roads and right-of-way areas were masked. Ground returns were classified for both datasets using a cloth simulation filter algorithm, which was selected due to implementation simplicity and demonstrated accuracy (Zhang et al. 2016). Digital surface models (DSM) and canopy height models (CHM) were interpolated from absolute and ground normalized return elevations respectively using pit-free algorithms due to reliability in producing smooth surfaces from high density point clouds (Khosravipour et al. 2014). DSMs and CHMs were generated at a cell size of 0.5 m, which was selected to capture local variation in canopy height without exceeding the capabilities of the SPL100 point density. All lidar point cloud processing steps in this letter were conducted using the lidR package in R (Roussel et al. 2020).

2.5. UAV-borne laser scanning vegetation structural index

To capture the variation in forest structure across the five sample areas, we derived a structural index (SI) from the ULS point clouds as a ratio of the return density (points/m^2) in the uppermost 25% of canopy height, and the lowest 25% of canopy height; derived in 1 m cells. We normalized this index by subtracting lower and upper canopy return densities on the numerator and summing density values on the denominator. Cells with negative values contained greater proportions of vegetation returns in the upper canopy relative to lower heights, which indicate areas with relatively dense upper canopies. Positive index values indicated areas where larger numbers of returns were produced from the lower portion of the forest's vertical profile. Positive cells were then associated with vertical configurations consistent with more porous, open canopy areas and well-spaced trees. We classified resulting SI values in four equal intervals from −1 to 1.

$$SI = \frac{(\text{ULS lower point density} - \text{ULS upper point density})}{(\text{ULS lower point density} + \text{ULS upper point density})}$$

2.6. Lidar signal attenuation depth estimation and distributions

To approximate the lidar signal attenuation of individual returns, we adapted an approach by Véga et al. (2016,) whereby individual absolute point elevations were subtracted from corresponding 0.5 m DSM values at a given location, this produced an estimated depth value within the canopy for each return. In our case, point level signal attenuation depths were normalized as percentages of canopy height by dividing each return depth residual by the associated CHM value of the given cell, allowing for comparison across forested sites with varying canopy heights. Distributions of signal attenuation depth values were binned across 20 equal intervals from the top of the canopy (0%) to the ground surface (100%). By representing binned frequencies as a proportion of total returns we were able to relate SPL100 and ULS point clouds despite around a 25× difference in the number of ULS returns per square metre. Relative binned frequencies from both platforms were grouped by corresponding structural index classes (Figure 1 and 2).

3. Results

ULS and SPL100 point clouds along with normalized height metrics for each plot are shown on Figure 1. Upper canopy lidar height metrics were relatively consistent between platforms although ULS produced higher values for max elevation and upper percentile values (e.g. zmax, zq95, zq80) across plots. Internal canopy metrics (zq25, zq05) varied between platforms; most evident in the birch plot where SPL100 penetration was considered to be most limited (Figure 1). In acquisition areas dominated by aspen, the ULS system produced larger proportions of returns from aspen stems potentially contributing to higher values for the 25th percentile of return heights in these plots. The open forest configuration plot dominated by black spruce showed greatest agreement between height metrics of both platforms.

3.1. Lidar signal attenuation depth distributions

Overall patterns across structural classes showed SPL100 consistently produced greater proportions of returns from the uppermost canopy depth bin with ULS returns more evenly distributed across mid-height bins. Trends reflect signal attenuation as well as actual vegetation structure present across canopy layers; differences in relative returns therefore allow for comparison between characterization by the two platforms.

Grid cells classified as open by the structural index (SI class 4) exhibited the greatest consistency in distributions of signal attenuation depth returns across the two platforms (Figure 2). A total of20.9% of SPL100 returns in these areas were recorded within the uppermost canopy height bin, whereas 10.9% of the total ULS returns were within this layer. In the mid-canopy layers (i.e. between 20–80% of canopy heights), the SPL100 data had between 3.0% and 4.7% of its total relative returns per bin. The ULS system produced an average of 16% greater proportion of returns within these mid-elevation bins relative to the SPL100 system. In the case of open structure, 32.7% of ULS returns were recorded from the lowest bins of the vertical foliage profile (80–100% of canopy height) compared to 27.3% of SPL returns.

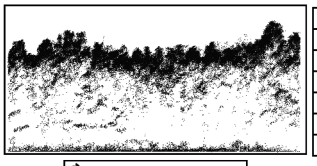

Metric	ULS Birch
zmax	13.7
zq95	8.8
zq80	8.0
zq25	6.6
zq05	0.5
% ground	1.1

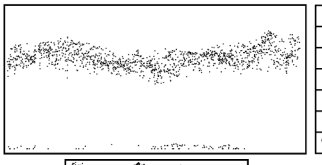

Metric	SPL Birch
zmax	11.7
zq95	8.2
zq80	7.6
zq25	6.5
zq05	5.6
% ground	1.4

Metric	ULS Aspen 1
zmax	36.4
zq95	34.3
zq80	32.8
zq25	6.6
zq05	0.5
% ground	0.6

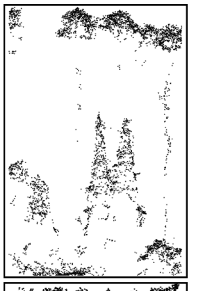

Metric	SPL Aspen 1
zmax	35.7
zq95	33.9
zq80	32.3
zq25	2.4
zq05	0.3
% ground	1.2

Metric	ULS Aspen 2
zmax	32.0
zq95	30.9
zq80	30.0
zq25	9.3
zq05	1.7
% ground	0.5

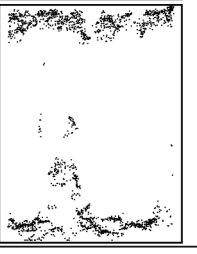

Metric	SPL Aspen 2
zmax	31.8
zq95	30.6
zq80	29.5
zq25	2.3
zq05	1.2
% ground	0.4

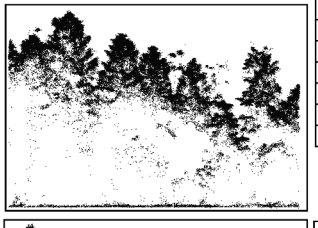

Metric	ULS Cedar
zmax	24.6
zq95	18.2
zq80	13.4
zq25	8.6
zq05	3.8
% ground	0.7

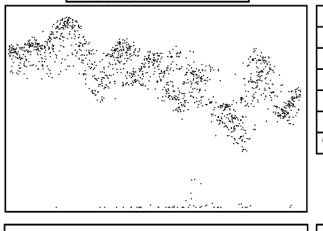

Metric	SPL Cedar
zmax	24.3
zq95	17.4
zq80	13.1
zq25	8.5
zq05	2.5
% ground	1.9

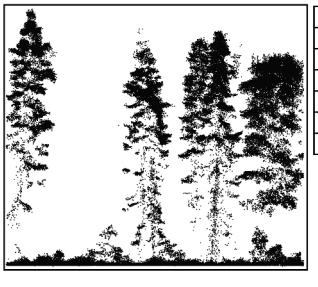

Metric	ULS Spruce
zmax	21.5
zq95	17.0
zq80	14.6
zq25	0.9
zq05	0.1
% ground	2.9

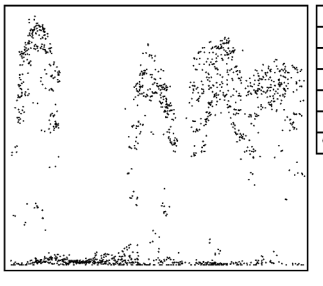

Metric	SPL Spruce
zmax	21.2
zq95	16.8
zq80	14.4
zq25	0.2
zq05	0.0
% ground	10.4

Figure 1. Two-metre-wide cross-section visualization of five ground normalized point clouds corresponding to plot sample areas (400 m^2) at centre of larger acquisitions. Individual ground normalized returns represented as points. Tables include lidar point cloud height metrics; maximum point elevation (zmax), 95th, 80th, 25th, and 5th quantile height values (zq95, zq80, zq25, zq05) as well as percentages of ground returns for plots from both platforms. ULS displayed on left, SPL100 on right.

The low-density structural class (SI class 3) had similar trends of agreement as the open class with SPL100 producing 26.7% of total returns from the uppermost bin of canopy depths relative to 20.0% by the ULS. 13.5% of ULS returns achieved depths between 5% and 20% of canopy height compared to SPL100 which produced 13.6% in these layers. Penetration to reveal mid-canopy structure (20–80% of CHM) was similar between

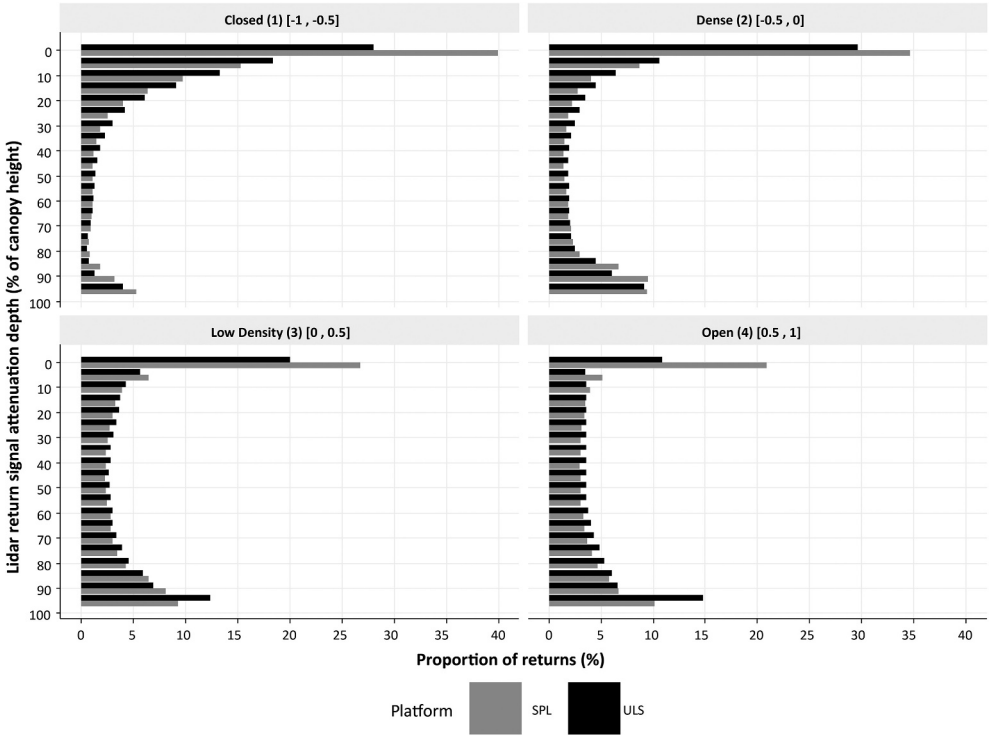

Figure 2. Relative distributions of lidar return signal attenuation depth values for SPL100 and ULS stratified by structural index class. SI class displayed in parentheses with range of included SI values in brackets. On the vertical axis, 0 indicates 'top' of canopy surface; with 100 indicating full penetration to the ground. Returns are binned in 5% intervals and displayed as relative proportions of total platform returns. Grey and black bars represent SPL100 and ULS platforms, respectively.

platforms in lower cover, with each depth bin containing between 4.5% and 2.6% of total returns for ULS and 4.2% and 2.3% for the SPL100. Both platforms had similar proportions of returns which fully penetrated canopy layers to produce returns from 90% to 100% depth of the canopy height: 25.1% for ULS and 23.8% for SPL100. Overall agreement between SPL100 and ULS was highest across penetration depths in the low-density and open structural classes.

In the intermediate dense structural class (SI class 2), 34.6% of SPL100 and 29.6% of ULS returns were recorded in the uppermost canopy height bin. The ULS system recorded 40.6% of its returns within the upper canopy (5–20% of CHM) compared to only 31.3% from SPL100. ULS returns more readily achieved mid canopy penetration depths (20–80% of CHM) with between 3.5% and 1.8% of ULS total returns recorded across these 12 penetration depth bins compare to SPL100 which had between 2.9% and 1.4% for the same interval. Penetration of lidar pulses to lower canopy depths (80–100%) was achieved by 22.2% of ULS returns in classified dense areas compared to 28.5% from SPL.

The closed density structural class (SI class 1) showed the greatest differences in ULS and SPL100 signal attenuation depth distributions as ULS returns were more evenly distributed across bins. Under closed structural conditions the greatest proportions of

returns from both platforms achieved little penetration with 39.9% of SPL100 and 29.6% of ULS total returns occurring within the uppermost 5% of canopy height. ULS more readily penetrated this uppermost layer to produce 40.6% of total returns within subsequent upper canopy bins (5–20% of CHM) relative to only 31.3% by the SPL100. Mid-canopy layers (20–80% of CHM) were more evenly characterized by ULS with each bin containing between 6.1% and 0.6% of total returns averaging 31% greater relative returns across these bins when compared to SPL100, which produced between 4.0% and 0.7% of total returns across these layers. Under closed conditions SPL100 did achieve full penetration (80–100% of CHM) for 11.0% of its returns compared to only 6.4% by the ULS.

4. Discussion

Researchers have already successfully applied SPL100 data to generate accurate enhanced forest inventories (EFI) using area-based approaches (Wästlund et al. 2018; Yu et al. 2020; White, Penner, and Woods 2021b). These approaches relate statistical properties of lidar point clouds (e.g. metrics) with measured plot level forest attributes to predict properties at a grid level across areas of lidar coverage (Coops 2015). Yu et al. (2020) compared SPL100 and Titan LML derived point clouds, and found increased cover penetration capability by the LML sensor while still noting general agreement across lidar height metrics. Yu et al. (2020) also noted that the agreement between SPL100 and LML derived point cloud metrics was not perfect, recommending calibration between datasets prior to operational applications whereby SPL100 and LML data were combined or where area-based models would be transferred from one dataset to another. Leaf-on and leaf-off SPL100 data have also been assessed for their capacity to accurately characterize the terrain surface across a range of forest conditions, with results suggesting adequate levels of accuracy for forest management applications; however, the accuracy of elevation models was found to vary with both the composition and configuration of forest vegetation (White et al. 2021a). White et al. (2021a) noted that certain forest types were associated with reductions in elevation accuracy, particularly forest stands associated with standing water or saturated soils (treed wetlands, cedar) and stands that have dense understory vegetation above the ground surface (black spruce); similar compositions to plot stands visually appearing to have reduced SPL penetration in this study (Figure 1).

While area-based analyses (e.g. EFI) and terrain model generation have been proven effective with SPL100, potential disparities identified in the characterization of mid-elevation vegetation surfaces may become relevant as future efforts capitalize on SPL100 data's high point density for finer scale forestry applications. Successful segmentation of understory trees for example may require minimum point densities (e.g. 170 points/m^2), which provide sufficient returns from lower canopy occluded trees to facilitate adequate differentiation from overstory vegetation (Hamraz, Contreras, and Zhang 2017). Similar relationships have been demonstrated between increased point densities and accuracy in modelling field measured understory structure (Campbell et al. 2018). Our results indicate that under the highest density forest structure class; SPL100 produced 31% fewer relative returns between 20% and 80% of canopy height when compared to the ULS system. SPL100 point clouds under dense forest configurations may contain limited numbers of returns necessary for applications which require lower canopy

information such as prediction of crown base heights, wildfire fuels, wildlife habitat, and above-ground biomass. Further analysis with SPL100 data is required to examine the potential impact of reduced penetration and sensor characteristics on the utility of SPL100 to estimate these attributes; especially under dense upper canopy configurations.

The driving factors behind observed differences in mid-canopy vegetation characterization are difficult to isolate as multiple factors including laser wavelength, sensor characteristics and post-processing may play a role. Hopkinson et al. (2016) assessed LML systems operated with both green and NIR lasers and noted that wavelength-dependent trends were observed including preferential sampling by the green laser of upper canopy regions, increased canopy attenuation, and reduced sampling of mid-height vegetation; these trends are consistent with the results from SPL100 reported herein. Mandlburger, Lehner, and Pfeifer (2019) visually compared the penetration capabilities of LML and SPL100 data in a forest context, concluding that LML achieved a greater pulse density and more ground returns. Mandlburger, Lehner, and Pfeifer (2019) also reported that the average number of returns per laser pulse was 1.84 for the LML compared to 1.06 for the SPL100; authors posited that aggressive noise filtering of the SPL100 data may have resulted in the removal of returns from the vegetation canopy.

While several authors have reported bias in the distribution of SPL returns towards the upper forest canopy (e.g. Li et al. 2016; Mandlburger, Lehner, and Pfeifer 2019), herein we demonstrate that there is similarity in the relative distributions of ULS and SPL100 returns in the uppermost (0–20%) and lowest portions (80–100%) of the canopy. These results are consistent with those reported in Yu et al. (2020), where the SPL100 data were found to have relatively larger proportions of returns from the top of the canopy and from near the ground surface, with fewer returns in the mid-canopy. Quantifying penetration as a ratio of lidar returns ≤2 m in height in to all returns, Yu et al. (2020) reported a strong level of agreement between SPL100 and LML data penetration ratios (R^2 coefficient of determination = 0.98), with penetration being 5% greater for the SPL100 on average. Whereas LML systems operate at high photon detection thresholds to reduce the impact of solar noise during daytime operations, given the highly sensitive detectors used in SPL100, the impact of solar noise can be significant and necessitates extensive post-processing. As described in Degnan (2016) and Gluckman (2016), the general algorithmic approach to noise filtering is multi-stage and operates on vertical height intervals or bins. Given the proprietary nature of the noise filtering algorithms, the degree to which such post-processing approaches could potentially result in the loss of actual surface returns from within specific regions of the vertical canopy profile is difficult to determine (Mandlburger, Lehner, and Pfeifer 2019; Brown, Hartzell, and Glennie 2020). Quantifying the impact of the aforementioned potential drivers of observed SPL100 signal attenuation would require detailed examination of SPL100 point clouds before and after filtering is applied.

The capacity of SPL100 data for forest applications has been demonstrated in the literature and trade-offs associated with specific applications such as terrain characterization (Li et al. 2016; White et al. 2021a) and area-based forest inventories (Wästlund et al. 2018;

White, Penner, and Woods 2021b; Yu et al. 2020) have been quantified. SPL100 offers acquisition efficiencies, particularly for large forest management areas, that can be important for operational programmes. As SPL100 data become more widely available, a more fulsome understanding of the potential and limitations of SPL100 technology becomes possible. Despite potential caveats of SPL100 technology, the benefits may likely outweigh potential reductions in canopy penetration and mid-height returns under dense conditions. The increased sensitivity associated with the SPL100 enables higher acquisition altitudes when compared to traditional LML systems in turn allowing larger swaths, greater overlap between flight lines, and uniform parameters during acquisition (Swatantran et al. 2016). Increased return densities and acquisition efficiencies enabled by SPL100's increased swath width compared to conventional lidar make it a desirable choice for future wide-area mapping efforts of forests with aerial lidar (Mandlburger, Lehner, and Pfeifer 2019; Yu et al. 2020).

5. Conclusion

Herein we demonstrated how a locally deployed ULS can provide valuable reference data to investigate and quantify the characteristics of nascent airborne systems deployed over large areas. Signal attenuation depth analyses allowed for the estimation of depth within canopy across tens of millions of lidar returns. Results indicated a decreased characterization of mid-canopy height vegetation by SPL100 relative to the LML sensor under the densest forest structural conditions.

Acknowledgments

We would like to thank Richard Borger, Matthew Shelley, and field and UAV assistants from Mohawk college in Hamilton, Ontario who provided and operated the ULS system in the RMF to obtain reference data. Our additional thanks to the reviewers and editors involved in the peer review of this letter.

Disclosure statement

No potential conflict of interest was reported by the authors.

Funding

This work was funded through the eFRI Accuracy Assessment and Change Update Approaches project (project number 18-2018) from Forestry Futures Trust Ontario awarded to Nicholas C. Coops and Grant McCartney.

ORCID

Nicholas C. Coops http://orcid.org/0000-0002-0151-9037

Data availability statement

The data that support the findings of this study are available from the corresponding author, [Irwin. L], upon reasonable request.

References

Brown, R., P. Hartzell, and C. Glennie. 2020. "Evaluation of SPL100 Single Photon Lidar Data." *Remote Sensing* 12 (4): 1–16. doi:10.3390/rs12040722.

Campbell, M. J., P. E. Dennison, A. T. Hudak, L. M. Parham, and B. W. Butler. 2018. "Quantifying Understory Vegetation Density Using Small-footprint Airborne Lidar." *Remote Sensing of Environment* 215: 330–342. doi:10.1016/j.rse.2018.06.023.

Coops, N. C. 2015. "Characterizing Forest Growth and Productivity Using Remotely Sensed Data." *Current Forestry Reports* 1 (3): 195–205. doi:10.1007/s40725-015-0020-x.

Degnan, J. J. 2016. "Scanning, Multibeam, Single Photon Lidars for Rapid, Large Scale, High Resolution, Topographic and Bathymetric Mapping." *Remote Sensing* 8 (11): 958. doi:10.3390/rs8110958.

Gluckman, J. 2016. "Design of the Processing Chain for a High-altitude, Airborne, Single Photon Lidar Mapping Instrument." *Laser Radar Technology and Applications XXI* 9832: 983203. doi:10.1117/12.2219760.

Hamraz, H., M. A. Contreras, and J. Zhang. 2017. "Forest Understory Trees Can Be Segmented Accurately within Sufficiently Dense Airborne Laser Scanning Point Clouds." *Scientific Reports* 7 (6770): 1–9. doi:10.1038/s41598-017-07200-0.

Hopkinson, C., L. Chasmer, C. Gynan, C. Mahoney, and M. Sitar. 2016. "Multisensor and Multispectral LiDAR Characterization and Classification of a Forest Environment." *Canadian Journal of Remote Sensing* 42 (5): 501–520. doi:10.1080/07038992.2016.1196584.

Khosravipour, A., A. K. Skidmore, M. Isenburg, T. Wang, and Y. A. Hussin. 2014. "Generating Pit-free Canopy Height Models from Airborne Lidar." *Photogrammetric Engineering and Remote Sensing* 80 (9): 863–872. doi:10.14358/PERS.80.9.863.

Leica. "SPL100 Single Photon Lidar Sensor". Accessed 18 March 2021. https://leica-geosystems.com/en-us/%20products/airborne-systems/topographic-lidar-sensors/leica-spl100

Li, Q., J. Degnan, T. Barrett, and J. Shan. 2016. "First Evaluation on Single Photon-Sensitive Lidar Data." *Photogrammetric Engineering and Remote Sensing* 82 (7): 455–463. doi:10.14358/PERS.82.7.455.

Mandlburger, G., H. Lehner, and N. Pfeifer. 2019. "A Comparison of Single Photon and Full Waveform Lidar." *ISPRS Annals of the Photogrammetry, Remote Sensing and Spatial Information Sciences* 4 (2/W5): 397–404. doi:10.5194/isprs-annals-IV-2-W5-397-2019.

Roussel, J., D. Auty, N. C. Coops, P. Tompalski, T. R. Goodbody, A. S. Meador, J. Bourdon, F. De Boissieu, and A. Achim. 2020. "lidR: An R Package for Analysis of Airborne Laser Scanning (ALS) Data." *Remote Sensing of Environment* 251: 112061. doi:10.1016/j.rse.2020.112061.

Stoker, J., Q. Abdullah, A. Nayegandhi, and J. Winehouse. 2016. "Evaluation of Single Photon and Geiger Mode Lidar for the 3D Elevation Program." *Remote Sensing* 8 (9): 767. doi:10.3390/rs8090767.

Swatantran, A., H. Tang, T. Barrett, P. Decola, and R. Dubayah. 2016. "Rapid, High-resolution Forest Structure and Terrain Mapping over Large Areas Using Single Photon Lidar." *Scientific Reports* 6: 1–12. doi:10.1038/srep28277.

Véga, C., J. P. Renaud, S. Durrieu, and M. Bouvier. 2016. "On the Interest of Penetration Depth, Canopy Area and Volume Metrics to Improve Lidar-based Models of Forest Parameters." *Remote Sensing of Environment* 175: 32–42. doi:10.1016/j.rse.2015.12.039.

Wästlund, A., J. Holmgren, E. Lindberg, and H. Olsson. 2018. "Forest Variable Estimation Using a High Altitude Single Photon Lidar System." *Remote Sensing* 10 (9): 1442. doi:10.3390/rs10091422.

White, J. C., M. Penner, and M. Woods. 2021b. "Assessing Single Photon LiDAR for Operational Implementation of an Enhanced Forest Inventory in Diverse Mixedwood Forests." *The Forestry Chronicle* 97 (01): 78–96. doi:10.5558/tfc2021-009.

White, J. C., M. Woods, T. Krahn, C. Papasodoro, D. Bélanger, C. Onafrychuk, and I. Sinclair. 2021a. "Evaluating the Capacity of Single Photon Lidar for Terrain Characterization under a Range of Forest Conditions." *Remote Sensing of Environment* 252: 112169. doi:10.1016/j.rse.2020.112169.

Yu, X., A. Kukko, H. Kaartinen, Y. Wang, X. Liang, L. Matikainen, and J. Hyyppä. 2020. "Comparing Features of Single and Multi-Photon Lidar in Boreal Forests." *ISPRS Journal of Photogrammetry and Remote Sensing* 168: 268–276. doi:10.1016/j.isprsjprs.2020.08.013.

Zhang, W., J. Qi, P. Wan, H. Wang, D. Xie, X. Wang, and G. Yan. 2016. "An Easy-to-Use Airborne LiDAR Data Filtering Method Based on Cloth Simulation." *Remote Sensing* 8 (6): 1–22. doi:10.3390/rs8060501.